2023 IEEE/ASME International Conference on Advanced Intelligent Mechatronics (AIM)
June 28-30, 2023. Seattle, Washington, USA

Multi-axis Manipulator Kinematic Calibration using a Novel Linearized Finite Screw Deviation Model

Jaehyung Kim, and Min Cheol Lee

Abstract— **This article proposes a method with a serial manipulator calibration technique using the linearized finite screw deviation model for calibrating the manipulator to reduce error in the workspace. With the emergence of robot technology, applications of the multi-axis manipulator have significantly increased. In previous research, many studies calibrated the multi-axis manipulator using end-effector tracking devices such as vision-sensor-based apparatus. However, the appliance of a special device for calibration can be resource-consuming in practical applications for applying every damaged manipulator. In this research, the proposed method helps the keep manipulator works appropriately in the workspace when the situation cannot afford those tracking devices because of the lack of resources such as budget and time. By designing a linearized finite screw deviation model to calculate the error of each axis of the manipulator from the non-continuous points trajectory of the end-effector, the error model becomes an affine function applicable in the global optimization method which can identify the deviation of the manipulator and leads to reduction of the error in the workspace. To validate the performance of the proposed method, simulation and the experiment were carried out with seven degrees of freedom manipulator.**

Index Terms— **Manipulator Calibration, Error Identification, Redundant manipulator, Finite screw**

I. INTRODUCTION

Multi-axis manipulator has allowed robots to perform numerous tasks in a complex environment as personal or professional service robots. In the research of the Korea Institute of Market Research [1] and the International Federation of Robotics [2], the growth of technology to assist robots is relatively slow respect to the annual installations of industrial robots is constantly increasing. More recently, calibration of the multi-axis manipulator is important for accurate and reliable control with increasing demands for articulated robots in the industrial field. In the kinematic calibration of the manipulator, researchers have progressed to the extent of the maintenance of robots [3]. Many calibration techniques were studied with end-effector continuous tracking devices such as laser trackers.

Several vision sensor-based (e.g., video recorder) techniques exist for the study of hand-eye manipulator calibration, Daniilidis *et al*. [4] introduced a calibration technique using a vision sensor and Levenberg-Marquardt minimization. They calibrated the manipulator by utilizing the dual quaternion and the recorded end-effector trajectory, assuming no error between the camera-identified end-effector position. Renaud *et al*. [5] proposed an online calibration technique using multiple cameras, where the manipulator was calibrated with model estimation using vision information from different angles. They demonstrated the calibration on a parallel robot, assuming no error in the camera-acquired information. Li *et al*. [6] developed a hand-eye calibration technique for grinding robots, utilizing posture information from a 3-D scanner. By calibrating the manipulator with the criterion sphere design, they achieved a 20% reduction in the mean error of the end-effector. Vision sensor-based hand-eye calibration offers advantages such as obtaining overall posture information and being cost-effective. However, it requires precise coordinate data of the manipulator obtained from pixel data, necessitating an error identification method to calibrate the camera's data warp. To enhance precision, some studies incorporated laser trackers to acquire more accurate end-effector trajectory data than what the camera provides. Park *et al*. [7] and To *et al*. [8] proposed transfer matrix-based iterative least-square methods for calibrating industrial manipulators with 6 Degrees of Freedom (DoF) and 4 DoF, respectively. Sun *et al*. [9], [10] introduced a finite screw-based product of the exponential (POE) method for calibration, utilizing a quasi-differential function. While laser trackers offer precise end-effector trajectory acquisition, they are costly and may require training, limiting their widespread applicability to damaged manipulators.

Vision sensors can be replaced with stereotactic apparatus. Veitschegger *et al*. [11] and Zhong *et al.* [12] applied a probe to indicate the position of the end-effector in calibration, He *et al.* [13], Zhuang *et al.* [14], and Escande *et al.* [15] applied potentiometer-based tracking device to record the trajectory of the end-effector. These stereotactic apparatus-based methods can measure the end-effector trajectory easily and precisely because of the manipulator and measurement device are physically connected, and easily accessible than laser tracker. Accordingly, this article proposes a method which requires non-continuous trajectory from stereotactic apparatus for ease of accessibility.

The calibration method can be divided into 2 categories: based on the local link coordinate system and the global coordinate system [16]. The advantage of the local link coordinate system-based calibration method is intuitive calculation. The global link coordinate system consists of zero-reference modelling [17] and the product of the exponential

This research was funded by Korea Institute of Machinery and Materials, (Project number: NK238A, 2022, Korea) and supported by the Korea Institute of Energy Technology Evaluation and Planning(KETEP) and the Ministry of Trade, Industry & Energy(MOTIE) of the Republic of Korea (No. 20214000000410).

Jaehyung Kim and *Min Cheol Lee are with the Department of Mechanical Engineering, Pusan National University, 635-4 Jangjeon-2 dong, Geumjeong-gu, Busan 609-735, South Korea (e-mail: 11045kjh@naver.com, mclee@pusan.ac.kr)

* Corresponding author.

(POE) formula[18], where the POE formula is based on finite motion. Each link of the manipulator is not connected to its adjacent link but is connected to the global coordinate. Therefore, the POE formula has extensive applicability. Focusing on these advantages, POE formula-based intuitive deviation model was designed in this article which can apply to a multi-axis manipulator. In finite screw theory [9], which is a branch of the POE-based method, differentiation of screw can be expressed with constraints: assuming there is no differentiation in the axis of rotation. These are also known as 'twist' [19]. In a practical application such as calibration, the rotation axis also deviates from the initial position by external disturbance such as collision. In this study, finite screw method based linear deviation model was designed, which enables the calculation about differentiation of successive finite screws from nonlinear complex calculation to linear affine function. By the model becomes an affine function, the proposed method can be easily applied to various optimization method.

This article proposes a multi-axis manipulator error calibration technique with a linearized finite screw deviation model. With only a few end-effector postures and their corresponding axis angles, the workspace error of the manipulator can be calibrated with a simple 3-D printed stereotactic apparatus, even if it has redundancy. The proposed method is based on finite screw theory [9], the powerful tool to establish the link structure of the manipulator from global coordinates. Moreover, a global optimization technique [20], [21] was applied to find an optimal solution that lies in a high-dimensional system, the affine function consisting of linear deviation. The main contributions of this study are as follows:

1. The novel linearized finite screw error model has been designed to the error model of the multi-axis manipulator, which allows the calculation of the deviation of the successive finite screw with an affine function of each finite screw differentiation. This enables point-based calibration calculation by global optimization method.
2. Without using the laser tracker or the potentiometer-based stereotactic apparatus, this study uses a simple 3-D printed end-effector for recording the coordinates to increase applicability. By applying the 3-D printed end-effector, the proposed method can design the deviation model and reduce the error in the workspace.
3. Simulation of the proposed method has been conducted to evaluate its efficiency. Furthermore, an experiment on a serial manipulator with redundancy has been conducted to validate the proposed method.

With these contributions, the proposed method allows the workspace calibration of the manipulator with non-continuous points. By optimizing the linearized finite screw deviation model, the error of the manipulator can be calibrated with only a few postures of the end-effector. Simulations and experiments with a 9-point poking action were conducted with a redundant manipulator, and circle drawing maneuver was also conducted to validate the performance of the proposed method.

II. Linearized Finite Screw Model of Multi-axis Manipulator

When formulating the error model of the end-effector generated by deviation of each axis, screw theory-based method has a great advantage is that the local coordinate system can be arbitrarily arranged on the corresponding link, which doesn't require successive calculations like the conventional transfer matrix-based method [16]. Similar to [22], linearization of the end-effector error model plays important role in identifying the deviation of axes. In this section, a linearized error model for calculating the actual axis model of the manipulator is proposed.

A. Screw Theory

In [9], finite screw can be described as semi-linear system. Screw theory can be divided to two categories:
The finite screw $S_f(\theta,l,\mathbf{s},\mathbf{r}) \in \Re^{6\times1}$, i.e., 'screw'.

$$S_f = \begin{bmatrix} a_{3\times1} \\ \beta_{3\times1} \end{bmatrix} = 2\tan(\theta/2)\begin{bmatrix} \mathbf{s} \\ \mathbf{r}\times\mathbf{s} \end{bmatrix} + l\begin{bmatrix} \mathbf{0} \\ \mathbf{s} \end{bmatrix} \tag{1}$$

In (1), $\mathbf{s} \in \Re^{3\times1}$ is the unit vector which denotes the direction of the rotation axis where the finite motion rotates around, $\mathbf{r} \in \Re^{3\times1}$ is the distance vector from origin of the space coordinates to rotation axis $\mathbf{s}$. θ and l are the amount of rotation and translation, respectively. $\alpha(\theta,\mathbf{s}) \in \Re^{3\times1}$ and $\beta(\theta,l,\mathbf{r},\mathbf{s}) \in \Re^{3\times1}$ are 1~3rd and 4~6th elements of finite screw S_f , respectively.

And the instantaneous screw $S_i(\dot{\theta},\dot{l},\mathbf{s},\mathbf{r}) \in \Re^{6\times1}$, i.e., 'twist'.

$$S_i = \dot{\theta}\begin{bmatrix} \mathbf{s} \\ \mathbf{r}\times\mathbf{s} \end{bmatrix} + \dot{l}\begin{bmatrix} \mathbf{0} \\ \mathbf{s} \end{bmatrix} \tag{2}$$

(2) represents instantaneous movement of the screw. In this article, S_i is called a 'unit screw' if $\dot{\theta}$ is 1 in (2).

To describe the finite motions with the composition of finite screws, a triangle product is used, which is shown in [10]

$$F = \begin{bmatrix} \alpha_a + \alpha_b + \widetilde{\alpha}_a\alpha_b/2 \\ \beta_a + \beta_b + (\widetilde{\alpha}_a\beta_b + \widetilde{\beta}_a\alpha_b)/2 \end{bmatrix}$$

$$G = \begin{bmatrix} \mathbf{0} \\ -(\tan(\theta_a/2)l_a\alpha_b + \tan(\theta_b/2)l_b\alpha_a)/2 \end{bmatrix} \tag{3}$$

$$H = 1 - \alpha_a{}^T\alpha_b/4$$

$$S_{f,ab} = \frac{F+G}{H} = S_b \Delta S_a \tag{4}$$

Where the operator "$\tilde{x}$" denotes 3×3 skew matrix of vector x , and the cross product "$\times$" in (3) is known as the screw product [23]. By using (4), the finite screw of the end-effector with successive axis can be calculated with the operator "Δ", which called the triangle product. [10]

$$S_{f,E} = S_n \Delta S_{n-1} \Delta \cdots \Delta S_2 \Delta S_1 \tag{5}$$

Where $S_{f,E}$ denotes finite screw of end-effector. To derive elements of screw from the product above, $\mathbf{s}$, $\mathbf{r}$, θ and l can be calculated as:

$$\begin{aligned} \mathbf{s} &= \frac{\alpha}{\| \alpha \|}, \ \theta = 2\text{atan}(\| \alpha \| /2) \\ \mathbf{r} &= \mathbf{s} \times (\beta - \mathbf{s}) / (2\tan(\theta/2)) \\ l &= [1/\mathbf{s}_1 \quad 1/\mathbf{s}_2 \quad 1/\mathbf{s}_3](\beta - 2\tan(\theta/2)(\mathbf{r} \times \mathbf{s}))/3 \end{aligned} \tag{6}$$

B. Differential of the finite screw

The partial differentiation of the triangle product can be linearized from (4) by assuming $l \cong 0$, which means there are almost no translational movement in finite screw.

$$\mathbf{M}_{\delta a}^{b} = \frac{4I_6 - 2\begin{bmatrix} \tilde{\alpha}_b & \mathbf{0} \\ \tilde{\beta}_b + \tan(\theta_b/2) l_b I_3 & \tilde{\alpha}_b \end{bmatrix} + S_{f,ab}[\alpha_b^T, 0]}{4 - \alpha_a^T \alpha_b} \tag{7}$$

$$S_{f,b} \Delta \delta S_{f,a} = \mathbf{M}_{\delta a}^{b} \delta S_{f,a}$$

$$\mathbf{M}_{a}^{\delta b} = \frac{4I_6 + 2\begin{bmatrix} \tilde{\alpha}_a & \mathbf{0} \\ \tilde{\beta}_a - \tan(\theta_a/2) l_a I_3 & \tilde{\alpha}_a \end{bmatrix} + S_{f,ab}[\alpha_a^T, 0]}{4 - \alpha_a^T \alpha_b} \tag{8}$$

$$\delta S_{f,b} \Delta S_{f,a} = \mathbf{M}_{a}^{\delta b} \delta S_{f,b}$$

The figure $\mathbf{M}$ denotes partial differential of triangle screw product where $S_{f,ab} = S_{f,b} \Delta S_{f,a}$. If the manipulator consists of n axes, the partial differentiation of (5) by m-th finite screw can be calculated using (7), (8) assuming no translational deviation of m-th finite screw.

$$\begin{aligned} (\delta S_{f,E})_m &= S_{f,n\sim m+1} \Delta \delta S_{f,m} \Delta S_{f,m-1\sim 1} \\ (S_{f,-(n\sim m+1)}) \Delta (\delta S_{f,E})_m &= \delta S_{f,m} \Delta S_{f,m-1\sim 1} \\ = \mathbf{M}_{\delta E,m}^{-(n\sim m+1)} (\delta S_{f,E})_m &= \mathbf{M}_{m-1\sim 1}^{\delta m} \delta S_{f,m} \end{aligned} \tag{9}$$

In (9), $S_{f,-(n\sim m+1)}$ denotes inverse finite screw of $S_{f,n\sim m+1}$, which satisfies $(S_{f,-(n\sim m+1)}) \Delta S_{f,n\sim m+1} = S_{f,n\sim m+1} \Delta (S_{f,-(n\sim m+1)}) = \mathbf{0}$. The inverse of finite screw can be easily calculated by inversing the sign of the $\mathbf{s}$ in the finite screw. The deviation of $S_{f,E}$ by m-th axis is shown as below:

$$(\delta S_{f,E})_m = (\mathbf{M}_{\delta E,m}^{-(n\sim m+1)})^{-1} \mathbf{M}_{m-1\sim 1}^{\delta m} \delta S_{f,m} \tag{10}$$

Finally, $\dot{S}_{f,E}$ can be obtained by combining the (10) of 1 ~ n-th axis, making a simple matrix form:

$$\begin{aligned} \delta S_{f,E} &\cong \sum_{i=1}^{n} (\delta S_{f,E})_i \\ &= \mathbf{M}_{n-1\sim 1}^{\delta n} \delta S_{f,n} + (\mathbf{M}_{\delta E,m}^{-(n\sim 2)})^{-1} S \delta_{f,1} + \sum_{i=2}^{n-1} ((\mathbf{M}_{\delta E,m}^{-(n\sim i+1)})^{-1} \mathbf{M}_{i-1\sim 1}^{\delta i} \delta S_{f,i}) \\ &= [(\mathbf{M}_{\delta E,m}^{-(n\sim 2)})^{-1}, \cdots, (\mathbf{M}_{\delta E,m}^{-(n\sim i+1)})^{-1} \mathbf{M}_{i-1\sim 1}^{\delta i}, \cdots, \mathbf{M}_{n-1\sim 1}^{\delta n}] \\ &\quad \cdot \left[\delta S_{f,1} \cdots \delta S_{f,m} \cdots \delta S_{f,n} \right] = \mathbf{M}^{\Sigma} \delta S_{f,\Sigma} \end{aligned} \tag{11}$$

In (11), $\mathbf{M}^{\Sigma} = [(\mathbf{M}_{\delta E,m}^{-(n\sim 2)})^{-1}, \cdots, (\mathbf{M}_{\delta E,m}^{-(n\sim i+1)})^{-1} \mathbf{M}_{i-1\sim 1}^{\delta i}, \cdots, \mathbf{M}_{n-1\sim 1}^{\delta n}]$, and $\delta S_{f,\Sigma} = [\delta S_{f,1} \cdots \delta S_{f,n}]$. By assuming each axis doesn't have translational properties, (11) can be changed to set of unit screws.

$$\mathbf{M}^{\Sigma} \delta S_{f,\Sigma} = \mathbf{M}^{\Sigma} \Theta_{\Sigma} \delta S_{i,\Sigma} \tag{12}$$

The $\Theta_{\Sigma} \in \Re^{6n \times 6n}$ in (12) is a diagonal matrix consisting set of $diag(2\tan(\theta/2)) \in \Re^6$ in diagonal order, which separates the $2\tan(\theta/2)$ from the deviation of the finite screw ($\delta S_{f,\Sigma} = \Theta_{\Sigma} \delta S_{i,\Sigma}$). By separating the term $\Theta_{\Sigma} \in \Re^{6n \times 6n}$, a set of finite screws becomes an unit screw [9].

If there are x number of $S_{f,E}$ and those axes share the same unit screw, the deviation of unit screws can be calculated as:

$$\begin{bmatrix} (\mathbf{M}^{\Sigma} \Theta_{\Sigma})_1 \\ \vdots \\ (\mathbf{M}^{\Sigma} \Theta_{\Sigma})_x \end{bmatrix} \delta S_{i,\Sigma} = \begin{bmatrix} \delta S_{f,E1} \\ \vdots \\ \delta S_{f,Ex} \end{bmatrix} + \mathbf{s} \tag{13}$$

The $\mathbf{s} \in \Re^{6x \times 1}$ is array of the slack variables from linearization.

III. Global Optimization Method

The finite screw error model has been linearized in previous chapter, the gap between the actual error model and the linearized model increases as the deviation becomes larger. This gap prevents to obtain optimal $\delta S_{i,\Sigma}$ with pseudo-inverse matrix of $\mathbf{M}^{\Sigma}$ from (13). Furthermore, yet error model has been linearized but still the dimension of $\delta S_{i,\Sigma}$ is $6n$ when there are n-axis in manipulator. However, if slack variable is given, the optimal $\delta S_{i,\Sigma}$ can be calculated by using the global optimization method. From genetic algorithms(GAs) [21],[24] to meta-heuristic algorithms[25], various global optimization method can be applied to (13). In this article, interior point method with particle-swarm method-based initialization was applied to optimize the $\delta S_{i,\Sigma}$. (13) can be affine if $\mathbf{s}$ is given but still complex because of a high-dimension feature. In this research, particle swarm optimization method with interior point method [29] was applied for optimizing the $\delta S_{i,\Sigma}$.

A. Interior point method

Interior point method, also referred to as barrier methods, was developed from Karush-Kuhn-Tucker (KKT) conditions [26]. In this study, the particle swarm optimization (PSO) method has been applied for initialization of interior point method[29]. The finite screw deviation model in (13) can be affine function with slack variable $\mathbf{s}$. Therefore, the optimization equation is designed as [28]:

$$\begin{bmatrix} (\mathbf{M}^{\Sigma}\Theta_{\Sigma})_1 \\ \vdots \\ (\mathbf{M}^{\Sigma}\Theta_{\Sigma})_x \end{bmatrix} = (\mathbf{M})_{\Sigma}, \quad \begin{bmatrix} \delta S_{f,E1} \\ \vdots \\ \delta S_{f,Ex} \end{bmatrix} = \delta S_{f,E\Sigma} \tag{14}$$

$$f(\delta S_{i,\Sigma}) = ((\mathbf{M})_{\Sigma}\delta S_{i,\Sigma} - \delta S_{f,E\Sigma})^T((\mathbf{M})_{\Sigma}\delta S_{i,\Sigma} - \delta S_{f,E\Sigma}) \tag{15}$$

$$\min(f(\delta S_{i,\Sigma})) \text{ , s.t, } g(\delta S_{i,\Sigma}) = |\delta S_{i,\Sigma}| \le b_{up} \tag{16}$$

In (16), $b_{up} \in \Re^{6x\times 1}$ (note that the x is number of axes in manipulator) is positive real vector that is a threshold of the $\delta S_{i,\Sigma}$. The b_{up} mostly determined from the rough measurement from the damaged manipulator.

The $f(x)$ can iteratively converge with a criterion (16), where iteration stops when (15) satisfies $f(x) \le \mathbf{s}^T\mathbf{s}$. Not only interior point method, but also other methods such as trust region method can be applied for convergence of (15). With a criterion (16), $\delta S_{i,\Sigma}$ can be optimized successfully by given slack variables $\mathbf{s}$ and b_{up}. However, the dimension of the (15) concerning $\delta S_{i,\Sigma}$ is significant when the number of the axis is high, especially when the manipulator is redundant. Without proper initialization, optimization may converge into local minima.

B. Particle swarm optimization method

Particle swarm optimization (PSO) method was applied for the initialization of the proposed method with (16). By simulating the behavior of particle swarms in nature, PSO starts with a random population and velocities with position [27], [30]. Each particle in the swarm represents potential solution, generated randomly within boundaries. After calculating each fitness value of each particle $\mathbf{x}^i(t) = \delta S_{i,\Sigma}(t)$ to initialize (16), then update the individual best with following equation:

$$\mathbf{x}^i(t) \in (b_{up}, b_{lo}), \ \mathbf{v}^i(t) \in (-|b_{up} - b_{lo}|, |b_{up} - b_{lo}|) \tag{17}$$

$$\mathbf{x}^i(t+1) = \mathbf{x}^i(t) + \mathbf{v}^i(t+1)$$

$$\mathbf{v}^i(t+1) = \mathbf{v}^i(t) + c_1 r_1 (p^i_{best} - \mathbf{x}^i(t)) + c_2 r_2 (g^i_{best} - \mathbf{x}^i(t)) \tag{18}$$

where $r_1, r_2 \in [0,1]$ are random parameters, and constants c_1, c_2 are acceleration parameters of PSO. Initialization of each particles position $\mathbf{x}^1(t)$ is generated within boundaries where $b_{lo} = -b_{up}$. The p^i_{best} is the fitness value of each particle in i-th iteration, and g^i_{best} is the best fitness value in the overall swarm [26]. Each fitness values are calculated with given value function of system, update $\mathbf{x}^i(t)$ and $\mathbf{v}^i(t)$ until termination criterion is met. After the termination, begin the interior point method with the calculated $\mathbf{x}^i(t)$.

IV. Simulation and Experiment

In the simulation and experiment, the end-effector of the damaged manipulator have a 9-points posture. After obtaining the axis angles corresponding with 9 points, apply them to the ideal manipulator model in simulation and get the corresponding end-effector posture. Finally, design the linearized finite screw deviation model with the proposed method and optimize the model to obtain the deviation of the damaged manipulator. Then calculate the 9-point trajectory corresponding to the calculated model using the trajectory generation method [31] and compare the ideal and calibrated end-effector postures for validating the proposed method.

A. Simulation with the redundant manipulator ROMAN-7

First, a simulation comparing the deviated finite screw with a 9-points end-effector posture was conducted. The deviation of each axis was applied randomly, applying the 9-point trajectory from the ideal configuration of the manipulator (initial points). In practical, multi-axis manipulator tilts in a similar direction because of gravity. Therefore, the deviation tends to be more significant as the axis is far from the base. In this simulation, a total of 100 manipulator configurations are randomly selected for calibration. The overall schematics of the simulation are shown in fig. 1. The simulation method follows as written above but evaluates the average reduction ratio with 100 iterations of simulations. The average normalized error reduction rate was 77% from fig. 3, point 7 ([-35,-10,0] cm point in fig. 2(a)).

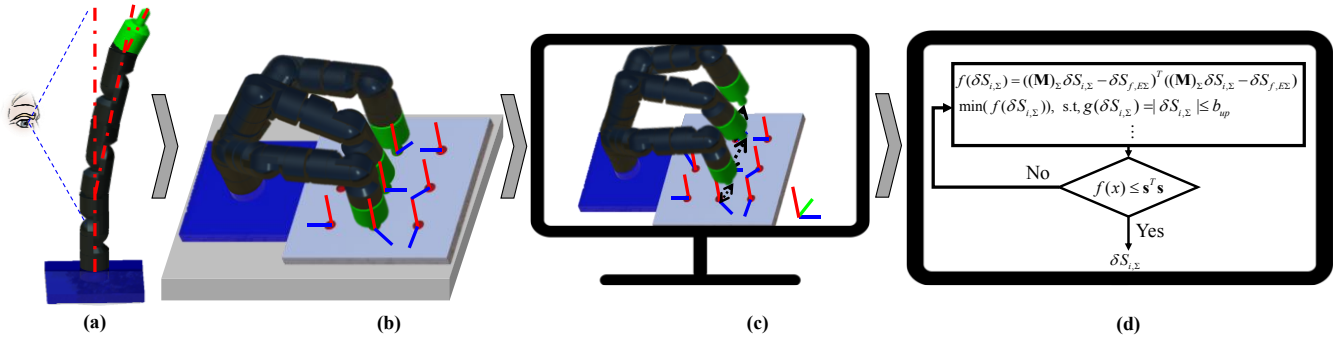

Fig. 1. Overall schematics of calibration with the proposed method. (a): acquiring the approximate shape, (b): obtaining the array of axis angles corresponding to desired end-effector posture, (c): simulating the manipulator with obtained angles, (d): identifying the deviation with the proposed method

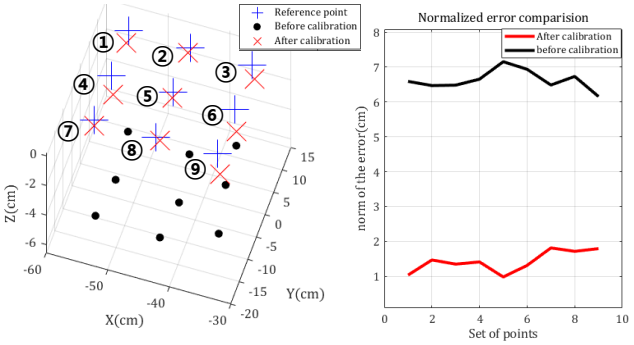

(a) (b)

Fig. 2. Manipulator error calibration comparison with proposed method in simulation example. (a): end-effector point comparison in cartesian coordinates. (b): Normalized error comparison of each point.

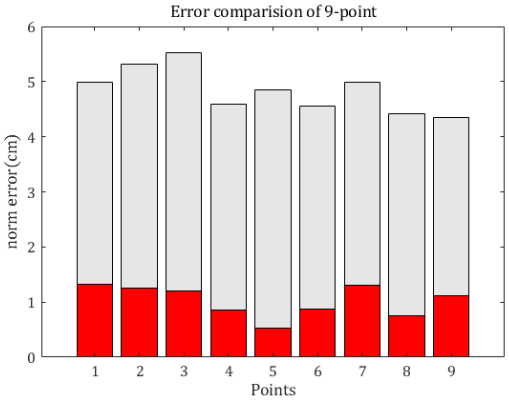

Fig. 3. Mean of normalized errors about 9-point (gray: before calibration, red: after calibration)

(a) (b)

Fig. 4. An experiment of the proposed method, (a): manual acquisition of axis angles corresponding to reference end-effector posture, (b): circle-trajectory drawing maneuver for comparison between with or without applying proposed-method

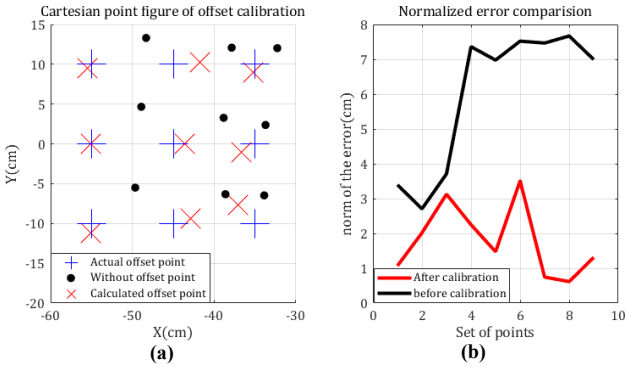

(a) (b)

Fig. 5. Manipulator error calibration comparison with proposed method with measured angles. (a): end-effector point comparison in cartesian coordinates. (b): error comparison of each point.

TABLE I
Trajectory comparison in the calibration experiment

Unit: cm	Reference trajectory	Before calibration	After calibration
Center position [x,y]	[-35, 0]	[-35.9, -0.8]	[-35.4. -0.3]
Tilt [degree]	0°	43.5°	17.5°
Horizontal axis	10	9.7	9.8
Vertical axis	10	10.6	10.2

B. Experiment with the redundant manipulator ROMAN-7

Second, the actual experiment with a 7-axis redundant manipulator was conducted. Control and communication system is the same as [31], which shares same manipulator with simulation. 3-D printed end-effector and posture target has been applied. By using a 3-D printed stereotactic apparatus, optical table and absolute encoder, axis angles corresponding to the reference end-effector posture from the damaged manipulator were obtained. As seen in fig. 4 (a), acquiring axis angle using stereotactic apparatus was carried manually by hand, 3-D printed apparatus, and optical table. The acquired axis angles were simulated and calibrated with proposed method. As shown in fig. 5, the proposed method was able to reduce the error in the workspace with calculated deviation. The average error reduction rate of fig. 5 (b) was 64.39%, which is less than a simulation result. After identifying the deviation of the manipulator axes using proposed method, measure the end-effector posture using another pen-attached 3-D printed end-effector device to determine whether the manipulator calibrated or not by apply the same reference trajectory and draw with or without calibration by proposed method. In the result, trajectory of the calibrated manipulator shows closer to the reference circle than before calibration as shown in fig. 6. The error of the center position and axes of the circle were reduced after calibration as seen in table 1. In the drawing maneuver, the small deformation on the pen attached part of the end-effector was observed. Without those additional variables, the result of experiment will be more precise as simulation.

V. Conclusion

This article aimed to reduce the error of the end-effector in the workspace by identifying the deviation of the damaged multi-axis manipulator from establishing a linearized finite screw deviation model. The performance of the proposed method was validated by simulation and experiment by showing the reduction of the error in the workspace without special devices such as a laser tracker. In the simulation, the error in the workspace was reduced by more than 77%. But in the experiment, the reduction rate was lower than the simulation

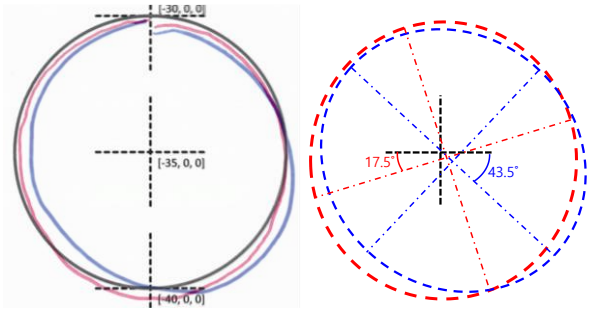

Fig. 6. The trajectory of the drawing maneuver in experiment, red: after calibration, blue: before calibration, (a): comparison of scanned trajectories, (b): refined trajectories with the computer aided design program

because of the tolerance of the 3-D printed end-effector to the occurrence of play in the encoder connection part due to the excessive use, which causes a minimal error at the acquired axis angles. If a precise global optimization method and firm stereotactic apparatus not like polylactic acid material are applied to the proposed method, the performance will increase more than the result of the experiment carried out in this study. Moreover, further research with additional optimization methods or with linear finite screw deviation models will be carried on for the calibration of complex manipulators such as redundancy or parallel connection.

REFERENCES

[1] S.W.Choi, "Market trends by field of robot industry, promising technology development and company status of 2023", KIMR

[2] World Robotics 2022, International Federation of Robotics,

[3] Z. Roth, B. Mooring and B. Ravani, "An overview of robot calibration," in IEEE Journal on Robotics and Automation, vol. 3, no. 5, pp. 377-385, Oct. 198

[4] K. Daniilidis and E. Bayro-Corrochano, "The dual quaternion approach to hand-eye calibration", Proceedings of 13th International Conference on Pattern Recognition, vol.1, pp. 318-322, Aug. 1996

[5] P. Renaud, N. Andreff, J.M. Lavest and M. Dhome, "Simplifying the kinematic calibration of parallel mechanisms using vision-based metrology," in IEEE Transactions on Robotics, vol. 22, no. 1, pp. 12-22, Feb. 2006

[6] W. -L. Li, H. Xie, G. Zhang, S. -J. Yan and Z. -P. Yin, "Hand–Eye Calibration in Visually-Guided Robot Grinding," in IEEE Transactions on Cybernetics, vol. 46, no. 11, pp. 2634-2642, Nov. 2016

[7] I. W. Park, B. J. Lee, S. H. Cho, Y. D. Hong and J. H. Kim, "Laser-Based Kinematic Calibration of Robot Manipulator Using Differential Kinematics," in IEEE/ASME Transactions on Mechatronics, vol. 17, no. 6, pp. 1059-1067, Dec. 2012

[8] M. To and P. Webb, "An improved kinematic model for calibration of serial robots having closed-chain mechanisms," Robotica, vol. 30, no. 6, pp. 963–971, 2012

[9] T. Sun, S. Yang and B.Lian, "Finite and instantaneous screw theory in robotic mechanism", springer, 2020

[10] T. Sun, C. Liu, B. Lian, P. Wang and Y. Song, "Calibration for Precision Kinematic Control of an Articulated Serial Robot," in IEEE Transactions on Industrial Electronics, vol. 68, no. 7, pp. 6000-6009, Jul. 2021

[11] W. K. Veitschegger and C. H. Wu, "Robot calibration and compensation," in IEEE Journal on Robotics and Automation, vol. 4, no. 6, pp. 643-656, Dec. 1988

[12] X.L. Zhong, J. M. Lewis and F.L.N.Nagy, "Autonomous robot calibration using a trigger probe", Robotics and Autonomous Systems, Vol.18, No.4, pp.395-410, 1996

[13] R. He, X. Li, T. Shi, B. Wu, Y. Zhao, F. Han, S. Yang, S. Huang, and S. Yang, "A kinematic calibration method based on the product of exponentials formula for serial robot using position measurements," Robotica, vol. 33, no. 6, pp. 1295–1313, 2015

[14] H. Zhuang, Z. S. Roth and F. Hamano, "A complete and parametrically continuous kinematic model for robot manipulators," in IEEE Transactions on Robotics and Automation, vol. 8, no. 4, pp. 451-463, Aug. 1992

[15] C. Escande, T. Chettibi, R. Merzouki, V. Coelen and P. M. Pathak, "Kinematic Calibration of a Multisection Bionic Manipulator," in IEEE/ASME Transactions on Mechatronics, vol. 20, no. 2, pp. 663-674, Apr. 2015

[16] C. Gang, L.Tong, C.Ming, J.Q. Xuan and S.H. Xu, "Review on kinematics calibration technology of serial robots", International journal of precision engineering and manufacturing, vol. 15, no. 8, pp. 1759-1774, Aug. 2014

[17] K.C.Gupta. "Kinematic Analysis of Manipulators Using the Zero Reference Position Description". The International Journal of Robotics Research, Vol.5, No.2, pp.5-13, 1986

[18] F. C. Park, "Computational aspects of the product-of-exponentials formula for robot kinematics," in IEEE Transactions on Automatic Control, vol. 39, no. 3, pp. 643-647, Mar. 1994

[19] K.M.Lynch and F.C.Park, "Modern Robotics. Mechanics, Planning, and Control." Cambridge U. press, 2017.

[20] J. Kennedy and R. Eberhart, "Particle swarm optimization," Proceedings of ICNN'95 - International Conference on Neural Networks, pp. 1942-1948, 1995

[21] D.P.Solomatine, "Genetic and other global optimization algorithms-comparison and use in calibration problems", proceedings of 3rd international conference on hydroinformatics, 1998

[22] A. Cibicik and O. Egeland, "Kinematics and Dynamics of Flexible Robotic Manipulators Using Dual Screws," in IEEE Transactions on Robotics, vol. 37, no. 1, pp. 206-224, Feb. 2021

[23] J.M. Hervé, The Lie group of rigid body displacements, a fundamental tool for mechanism design. Mech Mach Theory, vol. 34, no. 5, pp. 719–730, 1999

[24] D. E. Goldberg, "Genetic algorithms in search, optimization and machine learning, 13th edition", Addison-Wesly publishing company, 1989

[25] Z. Abdel, M. Ismail and S. El-Sayed. "A Survey on Meta-heuristic Algorithms for Global Optimization Problems". Journal of Intelligent Systems and Internet of Things. vol.8, no.2, pp.48-60, 2020

[26] P. A. Absil, A. L. Tits," Newton-KKT interior-point methods for indefinite quadratic programming". Computational Optimization and Applications, no. 36, pp. 5–41, 2007

[27] S. Arora and S.Singh. Butterfly optimization algorithm: a novel approach for global optimization. Soft Computing. Vol. 23, No. 3, 2019

[28] R. H. Byrd, J. C. Gilbert, and J. Nocedal. "A Trust Region Method Based on Interior Point Techniques for Nonlinear Programming." Mathematical Programming, vol 89, no. 1, pp. 149–185, 2000

[29] M. A. El-Shorbagy, Z. M. Hendawy, and A. A. El-Sawy, "Trust region-particle swarm for multi-objective engineering component design problems", Journal of global research in mathematical archives, vol. 1, no. 2, Feb. 2013

[30] M. R. Bonyadi and Z. Michalewicz, "Particle Swarm Optimization for Single Objective Continuous Space Problems: A Review," in Evolutionary Computation, vol. 25, no. 1, pp. 1-54, March 2017

[31] J. Kim, W. Jie, H. Kim, and M. C. Lee, Modified configuration control with potential field for inverse kinematic solution of redundant manipulator, vol. 26, no. 4. Aug. 2021

Jaehyung Kim is currently working toward the Ph.D. degree in mechanical engineering from Pusan National University, Busan, South Korea. His research interests include intelligent robot control, kinematics, machine learning, autonomous robots and simulation.

Min Cheol Lee received his Ph.D. degree in Applied Physics from the University of Tsukuba, Tsukuba, Japan in 1991. From 1991 to present, he has been a Professor wi th the School of Mechanical Engineering, Pusan National University, South Korea. His research interests include intelligent robot control, sliding mode control.